Conversions of Localized Excess Electrons and Spin States under External Electric Field: Inter-Cage Electron-transfer Isomer $(C_{20}F_{20})_3$&K_2

Jia-Min Tang,[a] Yin-Feng Wang,*[a] Qin Tian,[a] Xue-Xia Liu,[a] Zhijun Wang,[a] Jiangen Huang,[a] Hua-Rong Zhang,*[b] Kai Yang,[a] and Zhi-Ru Li*[c]

[a] Dr. Y.-F. Wang, Bs. Q .Tian, Dr. X.-X. Liu, Dr. Z. Wang.
Jiangxi Province Key Laboratory of Coordination Chemistry, School of Chemistry and Chemical Engineering,
Jinggangshan University
Ji'an, Jiangxi 343009 (P.R. China)
E-mail: cyclont@yeah.net

[b] Dr. H.-R. Zhang
Key Laboratory of Organosilicon Chemistry and Material Technology,
Hangzhou Normal University,
Hangzhou, Zhejiang 311121 (P.R. China).
E-mail: zhanghuaxy99@hznu.edu.cn

[c] Prof. Z.-R. Li
Institute of Theoretical Chemistry, Laboratory of Theoretical Computational Chemistry
Jilin University
Changchun 130023 (P.R. China)
E-mail: lzr@jlu.edu.cn

Abstract: By doping two potassium atoms among three $C_{20}F_{20}$ cages, peanut-shaped single molecular solvated dielectron $(C_{20}F_{20})_3$&K_2 was theoretically presented. The triplet structures with two excess electrons individually inside left and middle cages (isomers **I** or **II**) are thermodynamically more stable than both open-shell (OS) and close-shell (CS) singlet ones with lone pair of excess electrons inside middle cage. Applying an oriented external electric field (OEEF) of -20×10^{-4} au (-0.1018 V/Å) or a larger one can result in both left-to-right transfers of the two excess electrons, and then releasing the OEEF can form new kind of inter-cage electron-transfer isomers (**III** or **IV**). Each triplet **I** ~ **IV** with three redox sites may be new members of mixed-valent compounds, namely, Robin-Day Class II. For electrified **I** of $(C_{20}F_{20})_3$&K_2, the following spin states are ground state: 1) triplet state in field ranges of $-120 \times 10^{-4} < F_x < -30 \times 10^{-4}$ au and $30 \times 10^{-4} < F_x < 111 \times 10^{-4}$ au; 2) CS singlet state in range of F_x 111×10^{-4} and $\le -120 \times 10^{-4}$ au; 3) OS singlet state in ranges of $-30 \times 10^{-4} \le F_x \le -5 \times 10^{-4}$ au and $5 \times 10^{-4} \le F_x \le 30 \times 10^{-4}$ au.

Introduction

Recently, theoretical design of new high-performance molecular switching materials driven by oriented external electric field (OEEF) have witnessed large developments in the field of molecular electronics.[1-6]

As a simplest kind of extremely reactive intermediate, the investigation of the solvated electron plays a prominent role in physics, chemistry, and biochemistry.[7-15] For example, Adhikari et al have reported efficient capture of presolvated electrons by DNA base.[11] Also, for the charge- and electron-transfer transitions, manipulation of one or several electrons at molecular level remains a highly challenging task.[6,16,17] They have utmost importance in related fields of molecular electronics,[18] artificial photosynthesis,[17,19] molecular switches,[17,20] quantum-dot cellular automata (QCA),[21-23] solar cells,[24] and supramolecular assemblies.[25] As solvated electron systems (excess electron inside molecular cluster or cage) have not enough stabilities,[15] improving their stabilities is an important task.

To improve stabilities of general solvated electrons, we had turned our attention to encapsulation of electron(s) inside perfluorinated fullerene. For the perfluorinated fullerene, the $C_{20}F_{20}$ has been obtained experimentally.[26] Scuseria et al.[27] pointed out that the synthesis difficulty of $C_{60}F_{60}$ comes from the thermodynamic forces against it. However, the theoretical interests on the potential $C_{60}F_{60}$ cage[28] and relative $Ge_{60}F_{60}$ cage[29] are continuous. Very early, the smaller perfluorocyclobutane C_4F_8 and its radical anion $C_4F_8^-$ have been obtained experimentally.[30] Basing on the synthesized $C_{20}F_{20}$ and potential C_nF_n (n=20, 28, 36, 50, 60, and 80) cages, we have constructed a series of interesting cage-like single molecular solvated (di)electron systems with large stabilities: $e@C_{60}F_{60}$, $e_2@C_nF_n$ (n=20, 28, 36, 50, 60, and 80), $e@C_{20}F_{18}(NH)_2C_{20}F_{18}$, and $e@C_{24}F_{22}(NH)_2C_{20}F_{18}$.[31-36] These perfluorinated cages are efficient excess electron's containers. For these cages, the dipole moments of all the exo polarized $C^{\delta+}$-$F^{\delta-}$ bonds of each cage are directed toward the center of the cage to form an interior electronic attractive potential (IEAP) which can help to trap excess electron(s) inside these cages. These single molecular solvated (di)electron systems can provide a base of molecular electronics device. Basing on our $e@C_{20}F_{18}(NH)_2C_{20}F_{18}$, Ma et al., have successfully suggested a new type of molecular quantum-dot cellular automata (MQCA) candidate.[22,23] Recently, Li et al.,[37] have constructed new kind of electride molecular salts $e@C_{20}F_{19}(CH_2)_4NH_2...Na^+$ as novel, potential high-performance NLO materials. Also, basing on triple-cage-like electride salt $K^+[e@3C_8(O)]^-$, Li et al., also suggested[38] that multicage strategy is effective to enhance nonlinear optical (NLO) response.

Fifty years ago, Robin and Day introduced the systematic basis upon which all mixed-valence complexes are classified.[39]

In the first designed mixed-valence complexes, which were prepared by Creutz and Taube,[40] the mixed-valence ion is known as by Creutz-Taube ion. In recent years, there has been particular interest in the sometimes vague boundary between weakly localized (class II) and fully delocalized (class III) systems. Meyer et al discussed the localized-to-delocalized transition in mixed-valence chemistry, and proposed the defining characteristics of a new class of mixed-valence complexes, namely, class II–III.[41] For intervalence charge-transfer systems, novel donor–acceptor systems have been reported, particularly those based on purely organic species and those at the borderline between Class II and III.[42,43] For the double-cage-like single molecular solvated single electron systems $e^-@C_{20}F_{18}(NH)_2C_{20}F_{18}$,[33-35] the excess electron can be trapped inside different cages to form interesting Robin–Day-type inter-cage electron-transfer isomers.[33] In this case, besides the double-cage-like single molecular solvated electron systems,[31-35] We are interesting in the influence of the number of cage units on the localizations and spin states of two excess electrons. Especially, can the interesting Robin–Day-type inter-cage electron-transfer isomers also exist?

Recently, Sadlej-Sosnowska has reported that, in an uniform OEEF, a reversible switching between the two configurations of Li-benzene complex with significant dipole moments took place.[44] Straka et al demonstrated for MX@C_{70} (M: metal, X: nonmetal) systems that the relative orientation of enclosed MX with respect to a set of electrodes connected to the system can be controlled by application of OEEF(s).[2] For double-cage-like single molecular solvated electron systems of $e@C_{20}F_{18}(NH)_2C_{20}F_{18}$, and $e@C_{24}F_{22}(NH)_2C_{20}F_{18}$,[33-34] we have also used an external electric field to realize the inter-cage excess electron transfer and isomerization among three inter-cage electron transfer isomers. These will provide an approach for the manipulating localization(s) and spin state(s) of the excess electron(s) in multi-cage-shaped solvated dielectron systems by using external electric field.

In this paper, by doping two potassium atoms among three $C_{20}F_{20}$ cages, our investigation aims at obtaining the structures, excess electron localizations, and inter-cage excess electron transfers of the peanut-shaped single molecular solvated dielectron systems of $(C_{20}F_{20})_3\&K_2$, revealing the influence of the number of cage units on the localizations and spin states of two excess electrons, exhibiting stability of them under the external electric field, and suggesting the possible candidate for the new kind of Robin–Day-type inter-cage electron-transfer isomers.

Results and Discussion

Geometrical characteristics and inter-cage electron-transfer isomers

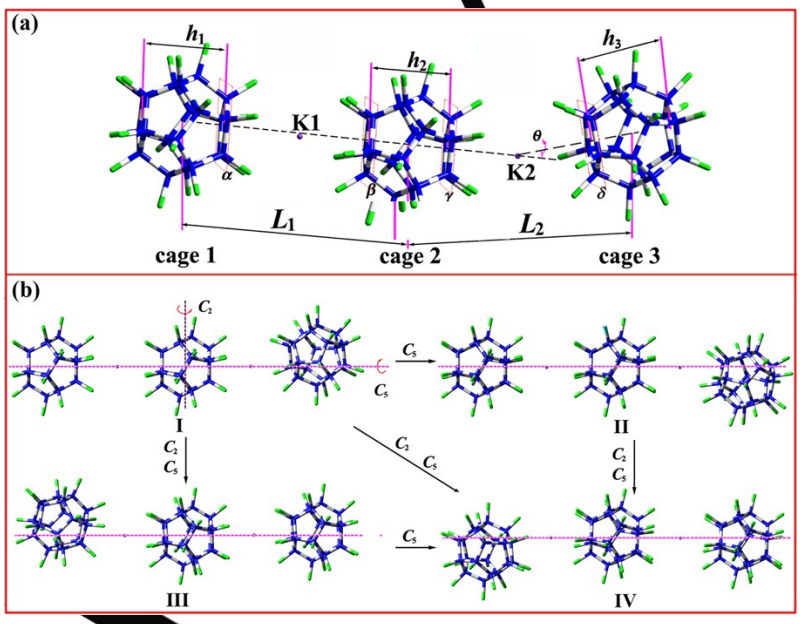

Figure 1. Optimized geometries of $(C_{20}F_{20})_3\&K_2$. (a) isomer **I**, (b) rotation operations among isomer **I**, **II**, **III**, and **IV**.

The optimized geometries with all real frequencies of $(C_{20}F_{20})_3\&K_2$ were shown in Figure 1. The selected structural parameters in closed-shell singlet (CS), open-shell singlet (OS), and triplet states were listed in Table 1. For both singlet (CS and OS) and triplet structures (T), the $(C_{20}F_{20})_3\&K_2$ represents face-to-face stacked $C_{20}F_{20}$ cages connected by two doped K atoms. From Figure 1, for the plane where five-membered carbon ring is located, the plane α of cage **1** and plane β of cage **2** are staggered with very small dihedral angle (0.55 (CS), 0.52 (OS) or 0.26°(T)). The similar situation happens between the five-membered plane γ (cage **2**) and δ (cage **3**) but some larger dihedral angle between them (15.08 (CS), 15.14 (OS), and 15.55°(T)).

The different sizes of three cages (**1**, **2**, and **3**) are closely related to excess electron localization(s) in both states (S and T). Results in Table 1 exhibit that cage **2** is the smallest one among three cages (h_2 (**2**) < h_1 (**1**) ≈ h_3 (**3**)) in singlet structures (both CS and OS), and both cage **2** (h_2) and **1** (h_1) are smaller in size than cage **3** (h_3) for triplet one. In addition, for both states (S and T), the centers of both cages **1** and **2** are in the K-K line (a

quasi C_5), while that of cage **3** slightly deviates (θ) from the K-K line. Considering this deviation, there may be some near-energy isomers due to different cage deviations. Three other structures with different cage deviations (isomer **II**, **III**, and **IV**, see Figure 1) from that of above one (isomer **I**, see Figure 1) have been found. Notice that, **II**, **III**, and **IV** can be obtained through rotation operations of **I** along the C_2 or C_5 axes. Therefore, **I**, **II**, **III**, and **IV** are not near-energy but equal-energy isomers with different cage deviations.

Table 1. Selected mean structural parameters of field-free **I** of $(C_{20}F_{20})_3\&K_2$.

	Singlet state		Triplet state (T)
	(CS)	(OS)	
h_1 (Å)	3.444	3.436	3.415
h_2 (Å)	3.375	3.394	3.402
h_3 (Å)	3.445	3.437	3.447
L_1 (Å)	9.583	9.573	9.577
L_2 (Å)	9.505	9.493	9.569
θ (°)	8.25	7.95	8.32
α & β (°)[a]	0.55	0.52	0.26
γ & δ (°)[a]	15.08	15.14	15.55

[a] Dihedral angle

For isomer **I**, results in Table 2 show that the natural popular analysis (NPA) charges of K1 and K2 atoms in field-free $(C_{20}F_{20})_3\&K_2$ are larger than 0.66 |e| for both singlet (CS and OS) and triplet (T) states, which indicates the valences of both K atoms are +1 for these states. At the same time, the NPA charge of cage **2** in CS singlet structure is -1.345 |e|, which indicates that valence of cage **2** in singlet structure is -2. For triplet one, the NPA charges of cage **1** and **2** are, respectively, -0.816 and 0.688 |e|, which suggests both valences of them are -1. Owing to open-shell characteristics, the NPA charge of cage **2** is only -0.890 |e| and that of both cages **1** and **3** are very small (-0.216 and -0.224 |e|) for OS singlet structure. Therefore, the 4s electrons of both K atoms are pulled out and trapped inside the fluorinated C_{20} cage(s) to form localized excess electrons due to the IEAPs for both singlet (CS and OS) and triplet (T) states.

Similar to isomer **I**, considering the rotation operation, the valence of cage **2** is -2 for singlet (CS or OS) **II**, **III**, and **IV.** Also, the valence of cages **1** and **2** for triplet **II** and that of cage **2** and **3** for triplet **III** and **IV** are -1.

Figure 2 gives the frontier molecular orbitals in both states and spin density distribution in triplet state of isomer **I**. The highest occupied molecular orbital (HOMO, see Figure 2a) in CS singlet state indicates that two excess electrons are trapped inside the middle smallest-sized $C_{20}F_{20}$ cage (**2**) with NPA charge of -1.345 |e| to form a lone pair of excess electrons. Also, the lone pair of excess electrons is trapped inside the middle smallest-sized $C_{20}F_{20}$ cage (**2**) for CS singlet isomers of **II**, **III**, and **IV** (see Figure S1).

Table 2. Natural popular analysis (NPA, |e|) charge and Dipole moments (μ_x, *D*) of **I** of $(C_{20}F_{20})_3\&K_2$ under different external electric fields (*EEFs*).

	Singlet state		Triplet state (T)
	(CS)	(OS)	
F_x = -120 × 10 $^{-4}$ au			
K1	0.710		0.708
K2	0.651		0.662
Cage **1**	0.157		0.165
Cage **2**	0.169		-0.636
Cage **3**	-1		-0.899
μ_x	8.77		104.96
F_x = -20 × 10 $^{-4}$ au			
K1	0.690	0.699	0.701
K2	0.646	0.677	0.687
Cage **1**	0.121	0.138	0.146
Cage **2**	-1.172	-0.830	-0.692
Cage **3**	-0.294	-0.685	-0.842
	22.16	43.71	18.93
F_x 0 au			
K1	0.664	0.664	0.678
K2	0.667	0.665	0.703
Cage **1**	0.007	-0.216	-0.816
Cage **2**	-1.345	-0.890	-0.688
Cage **3**	0.006	-0.224	0.122
	0.03	0.75	-35.20
F_x = 20 × 10 $^{-4}$ au			
K1	0.646	0.676	0.681
K2	0.693	0.700	0.709
Cage **1**	-0.298	-0.830	-0.825
Cage **2**	-1.167	-0.684	-0.693
Cage **3**	0.127	0.138	0.128
μ_x	-8.75	-43.92	-15.10
F_x = 111 × 10 $^{-4}$ au			
K1	0.645		0.833
K2	0.713		0.890
Cage **1**	-1.592		-1.173
Cage **2**	0.081		-0.612
Cage **3**	0.153		0.063
μ_x	-98.78		-97.99

For the OS singlet state, results in Figure 2b (HOMOα and HOMOβ) also suggest the two excess electrons are mainly trapped inside the middle smallest-sized $C_{20}F_{20}$ cage (**2**) with NPA charge of -890 |e| for isomer **I**. The small occupations of

the excess electrons inside end cages (**1** and **3**) are in accordance with the small NPA charge of both end cages (**1** and **3**). The similar condition happens to OS singlet isomers of **II**, **III**, and **IV** (see Figure S2).

From Figure 2c, the two single occupied molecular orbitals (SOMO1 and SOMO2) and spin density distribution of isomer **I** suggest one excess electron is confined inside the left $C_{20}F_{20}$ cage (**1**) with NPA charge of -0.816 |e| and the other one is confined inside the middle $C_{20}F_{20}$ cage (**2**) with NPA charge of -0.688 |e| for isomer **I**. Then, the two excess electrons are two single-excess-electrons and are, respectively, confined inside left (**1**) and middle cages (**2**) for triplet **I** of $(C_{20}F_{20})_3\&K_2$. The right largest-sized $C_{20}F_{20}$ cage (**3**) is empty for triplet **I** of $(C_{20}F_{20})_3\&K_2$. The sizes of the occupied $C_{20}F_{20}$ cage(s) are slightly smaller than that of the unoccupied one for both states, which shows that the occupations of electrons make the occupied cage slightly shrink. These are similar to that of the reported $e@C_{20}F_{18}(NH)_2C_{20}F_{18}$ and $e@C_{24}F_{22}(NH)_2C_{20}F_{18}$.[33,34] Considering the rotation operation, two single-excess-electrons are, respectively, confined inside left (**1**) and middle cages (**2**) for both isomers of **I** and **II**, while they are individually confined inside middle (**2**) and right cages (**3**) for both isomers of **III** and **IV** (see Figure S3).

Therefore, the lone pair of excess electrons is confined inside the middle smallest-sized $C_{20}F_{20}$ cage (**2**) for singlet **I**, **II**, **III**, and **IV** of $(C_{20}F_{20})_3\&K_2$, while two single-excess-electrons are, respectively, confined inside left and middle smaller-sized $C_{20}F_{20}$ cages (**1** and **2**) for triplet **I** or **II** of $(C_{20}F_{20})_3\&K_2$ and right and middle smaller-sized $C_{20}F_{20}$ cages (**2** and **3**) for triplet **III** or **IV** of $(C_{20}F_{20})_3\&K_2$.

Interestingly, all three $C_{20}F_{20}$ cages for $(C_{20}F_{20})_3\&K_2$ can trap excess electron(s) inside them, so they may be considered as three redox sites existing in the rare nonmetal mixed-valent (0, -1 and -2) molecule anion. Each isomer with three redox sites may be the founding member of a new class of mixed valence molecules, namely, nonmetal Robin-Day Class II-III. Singlet **I**, **II**, **III**, and **IV** of $(C_{20}F_{20})_3\&K_2$ with localized redox center (middle cage (**2**)) may be the founding members of Class II, while triplet **I**, **II**, **III**, and **IV** of $(C_{20}F_{20})_3\&K_2$ with delocalized redox centers may be the founding members of Class III. Similar to the reported $e@C_{20}F_{18}(NH)_2C_{20}F_{18}$ and $e@C_{24}F_{22}(NH)_2C_{20}F_{18}$,[33,34] isomers of both singlet and triplet $(C_{20}F_{20})_3\&K_2$ are Robin-Day-type inter-cage electron-transfer isomers.

Of course, different spatial localizations of the excess electrons lead to clearly different physical properties. For isomer **I**, from Table 2), the dipole moment component μ_x values are, respectively, 0.03 and -35.2 D for CS singlet structure with lone pair of excess electrons inside smallest-sized $C_{20}F_{20}$ cage (**2**) and triplet one with two single-excess electrons inside left and middle small-sized $C_{20}F_{20}$ cages (**1** and **2**). The μ_x value of OS singlet structure of isomer **I** is also close to zero. The difference of μ_x values between singlet (CS and OS) and triplet states is much considerable.

It is reported that for $e@C_{20}F_{18}(NH)_2C_{20}F_{18}$,[33] there exists a third structure with an excess electron equally confined in both $C_{20}F_{18}$ cages. Similarly, a triplet structure with D_{5d} point group of $(C_{20}F_{20})_3\&K_2$ has been found during our searching. This triplet D_{5d} structure shows that one excess electron is confined inside the middle $C_{20}F_{20}$ cage (**2**), and the other one is equally confined in both end $C_{20}F_{20}$ cage (**1** and **3**) (see Figure S4). However, this D_{5d} structure is a saddle point of fifth order due to five large imaginary frequencies.

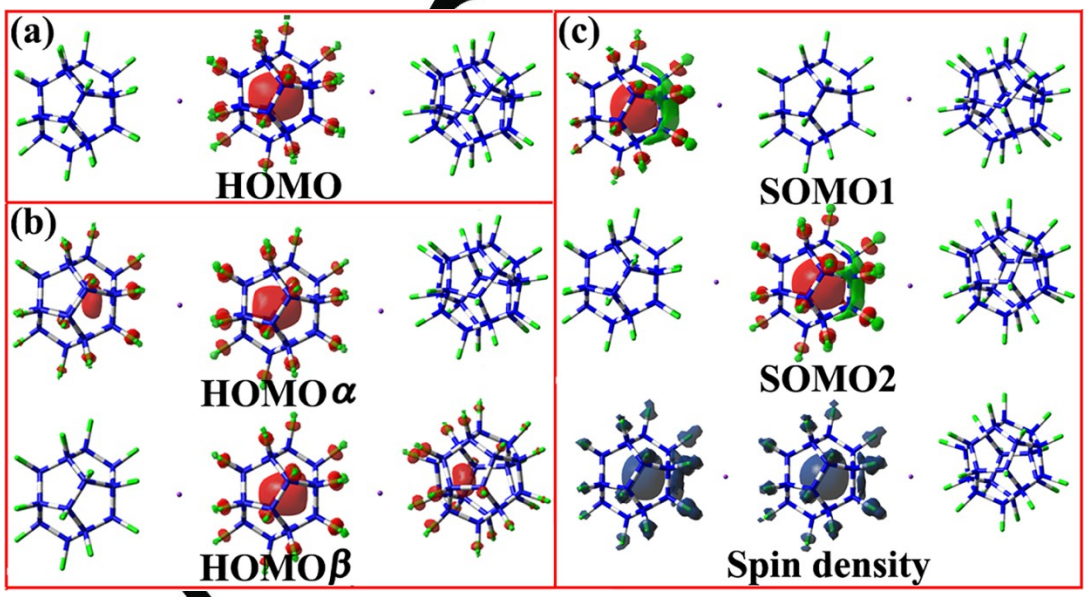

Figure 2. Selected frontier molecular orbitals (isovalue of 0.04 au) and spin density distribution (isovalue of 0.004 au) in different spin states of **I** of $(C_{20}F_{20})_3\&K_2$. a) CS singlet, b) OS singlet, and b) triplet state.

Inter-cage electron transfer isomerization

We have reported that application of OEEF of -10×10^{-4} au (-0.0514 V/Å) results in of an excess electron transfer from left to right cage of $e@C_{20}F_{18}(NH)_2C_{20}F_{18}$.[32] For singlet and triplet $(C_{20}F_{20})_3\&K_2$, the conversions of two excess electrons in three $C_{20}F_{20}$ cages are especially deserved studied. Results in Figure 3 ~ 5 and Table 2 give the evolutions of NPA charges of three cages (**1**, **2**, and **3**) of **I** of $(C_{20}F_{20})_3\&K_2$ under OEEFs.

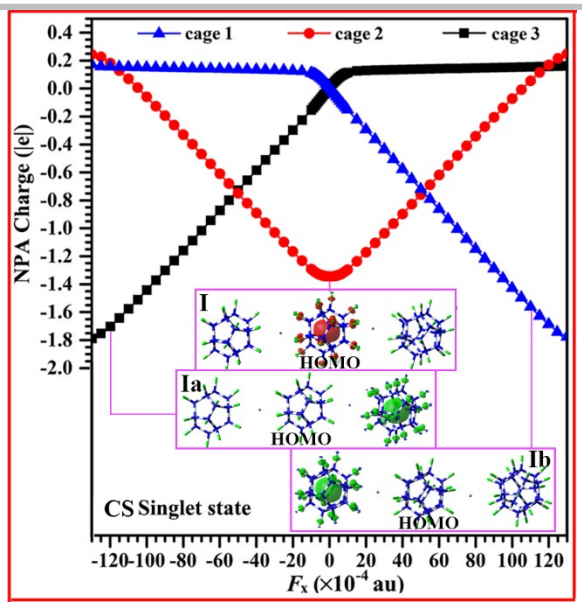

Figure 3. Evolution of NPA charges of CS singlet **I** of $(C_{20}F_{20})_3$&K_2. Molecular orbitals at the isovalue of 0.004 au.

For CS singlet **I** of $(C_{20}F_{20})_3$&K_2, from Figure 3, one can see that the absolute value of NPA charge of cage **2** decreases with increasing the intensity of OEEF in both positive and negative directions of x-axis (from F_x = 0 to 125 or -125 × 10^{-4} au). Simultaneously, the absolute value of NPA charge of cage **1** increases but that of cage **3** decrease as changing the intensity of OEEF in x-axis direction from F_x = -125 × 10^{-4} to 125 × 10^{-4} au. The NPA charge of cage **1** under F_x = 111 × 10^{-4} au (0.5705 V/Å) and that of cage **3** under F_x = -120 × 10^{-4} au (0.6168 V/Å) in CS singlet **I** of $(C_{20}F_{20})_3$&K_2 are, respectively, -1.592 |e| and -1.687 |e|. The HOMOs of CS singlet $(C_{20}F_{20})_3$&K_2 with and without F_x are also shown in Figure 3. From the analysis of HOMOs in Figure 3, the lone pair of excess electrons is confined inside the left $C_{20}F_{20}$ cage (**1**) under F_x = 111 × 10^{-4} au (0.5705 V/Å) and inside the right one (**3**) under F_x = -120 × 10^{-4} au (-0.6168 V/Å) for CS singlet **I** of $(C_{20}F_{20})_3$&K_2. Therefore, applying the OEEF of 111 × 10^{-4} au (0.5705 V/Å) and -120 × 10^{-4} au (-0.6168 V/Å) in the x-axis direction of singlet **I** of $(C_{20}F_{20})_3$&K_2 can result in the transfer of the lone pair of excess electrons from middle $C_{20}F_{20}$ cage (**2**) to left $C_{20}F_{20}$ cage (**1**) and from middle $C_{20}F_{20}$ cage (**2**) to right $C_{20}F_{20}$ cage (**3**), respectively. Then, the new OS singlet isomers of CS singlet **Ia** and **Ib** occur (see Figure 4). The μ_x value increases enormously when going from field-free singlet **I** of $(C_{20}F_{20})_3$&K_2 with lone pair of excess electrons inside middle $C_{20}F_{20}$ cage (**2**) to the electrified singlet **Ia** and **Ib** of $(C_{20}F_{20})_3$&K_2 with that inside end $C_{20}F_{20}$ cage (**1** or **3**). The isomerization of **II**, **III**, and **IV** are similar to that of **I**.

From Table 3, the diradical character value (y_0) of **I** of $(C_{20}F_{20})_3$&K_2 increases as increases the intensity of OEEF in both positive and negative directions of x-axis (from $|F_x|$ = 5 to 30 × 10^{-4} au) and then disappears suddenly under larger OEEF ($|F_x|$ > 30 × 10^{-4} au). The diradical character is remarkably weak for field-free OS singlet **I** of $(C_{20}F_{20})_3$&K_2, while that are much strong for electrified ones (5 × 10^{-4} ≤ $|F_x|$ ≤ 30 × 10^{-4} au). Different from the encapsulations of the two excess electrons inside the middle cage (**2**) of field-free OS singlet **I** of $(C_{20}F_{20})_3$&K_2, the NPA charges in Figure 4 and Table 2 indicate one excess electron is trapped inside the middle cage (**2**) and the other inside the end cage (**1** or **3**) as increases the intensity of OEEF in both positive and negative directions of x-axis (from $|F_x|$ = 5 to 30 × 10^{-4} au). The electric clouds of HOMOα and HOMOβ can provide support for this (see Figure 4). Then, new OS singlet isomers of OS singlet **Ia** and **Ib** occur. The encapsulations of the two excess electrons of OS singlet **Ia** and **Ib** are similar to that of triplet **III** and **I**, respectively (see Figure S3).

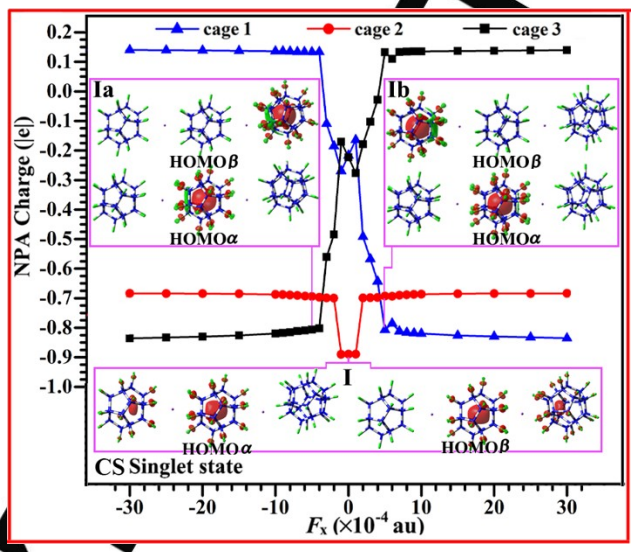

Figure 4. Evolution of NPA charges of OS singlet **I** of $(C_{20}F_{20})_3$&K_2. Molecular orbitals at the isovalue of 0.004 au.

Table 3. Evolution of diradical character (y_0) **I** of $(C_{20}F_{20})_3$&K_2 under OEEF (F_x, × 10^{-4} au).

Field	y_0	Field	y_0
-120	0.000	5	0.760
-35	0.000	10	0.827
-30	0.908	15	0.868
-25	0.899	20	0.891
-20	0.884	25	0.904
-15	0.860	30	0.913
-10	0.818	35	0.000
-5	0.747	40	0.000
0	0.094	111	0.000

For triplet **I** of $(C_{20}F_{20})_3$&K_2, from Figure 5 and Table 2, it can be found that both spin density and absolute value of NPA charge of cage **1** decrease but that of cage **3** increase with increasing the intensity of OEEF in negative directions of x-axis (from F_x = 0 to -40 × 10^{-4} au). The NPA charge of cage **1** under F_x = 0 au and that of cage **3** under F_x -20 × 10^{-4} au (-0.1018 V/Å) in triplet **I** of $(C_{20}F_{20})_3$&K_2 are, respectively, -0.816 |e| and -0.842 |e|. The SOMOs show that an excess electron is confined inside the left $C_{20}F_{20}$ cage (**1**) for triplet **I** of $(C_{20}F_{20})_3$&K_2 under F_x = 0 au but that is confined inside the right $C_{20}F_{20}$ cage (**3**) for triplet **I** of $(C_{20}F_{20})_3$&K_2 under F_x -20 × 10^{-4} au (-0.1018 V/Å). The encapsulations of the two excess electrons of electrified triplet **I** of $(C_{20}F_{20})_3$&K_2 (F_x = -20 × 10^{-4} au (-0.1018 V/Å)) (**III'**) are similar

to that of field-free triplet **III** of $(C_{20}F_{20})_3\&K_2$ (see Figure S3). Then, **III'** can change into **III** after releases the F_x and underdogs small deformations of both end cages.

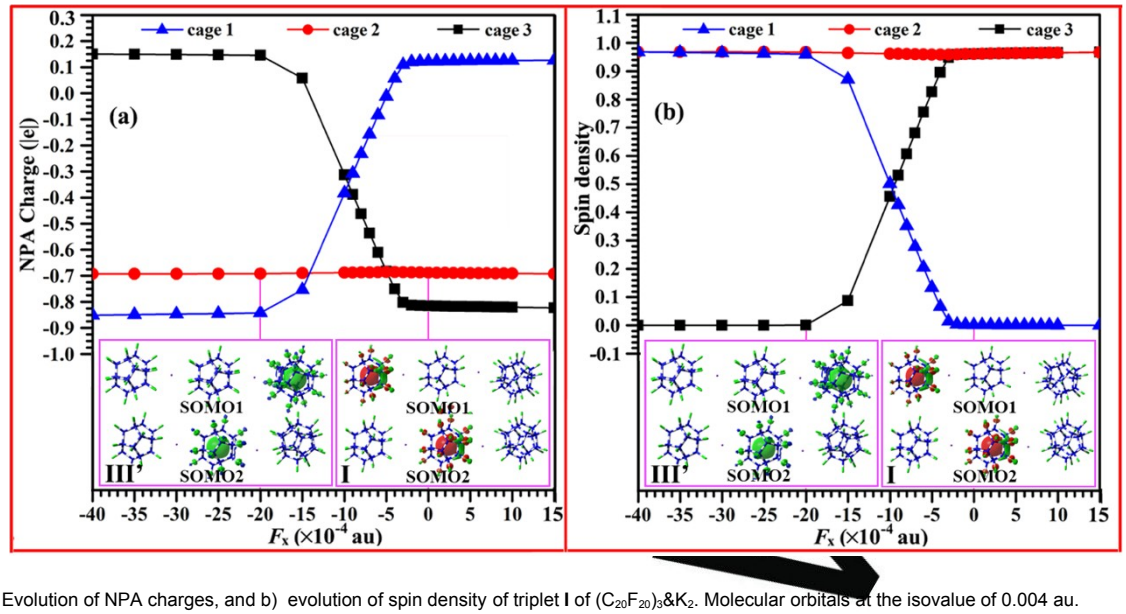

Figure 5. a) Evolution of NPA charges, and b) evolution of spin density of triplet **I** of $(C_{20}F_{20})_3\&K_2$. Molecular orbitals at the isovalue of 0.004 au.

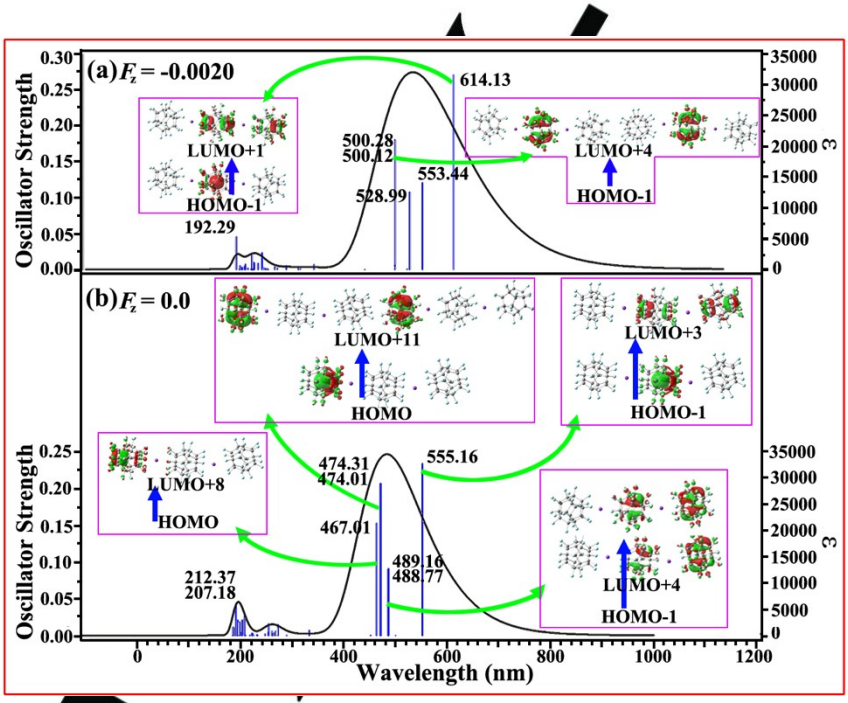

Figure 6. Excess electronic absorption spectra of triplet **I** of $(C_{20}F_{20})_3\&K_2$ at CIS/6-31G (d) level, a) F_z = -0.0020 au and b) F_z = 0.00 au. Molecular orbitals at the isovalue of 0.004 au.

Therefore, applying an OEEF of -20 × 10^{-4} au (-0.1018 V/Å) or larger one in the x-axis direction of field-free triplet **I** of $(C_{20}F_{20})_3\&K_2$ results in both left-to-right transfers of the two single-excess-electrons. The transfers of the excess electrons are exhibited that a single-excess-electron transfers from middle $C_{20}F_{20}$ cage (**2**) to right $C_{20}F_{20}$ cage (**3**) (**2** → **3**) and the other one transfers from right cage (**3**) to middle $C_{20}F_{20}$ cage (**2**) (**1** → **2**). For the single-excess-electron transfers, the electric field (F) work W can be estimated by the following formula:

$$W = Q_e F L \quad (1)$$

For both **1** → **2** and **2** → **3** electron transfers, Q_e = -1 and F = -0.0020 au. L = 9.577 (L_1) and 9.569 Å (L_2, see Table 1), respectively. So, W is 45.4 kcal/mol for both electron transfers.

Figure 6 gives the excess electronic absorption spectra of triplet **I** of $(C_{20}F_{20})_3\&K_2$ at CIS/6-31G (d) level with F_z = -0.0020 au and F_z = 0.00 au. From Figure 6, the maximum absorption peak (λ_{max}) is an inter-cage s → p transition for both field-free and electrified (F_z = -0.0020 au) triplet **I** of $(C_{20}F_{20})_3\&K_2$. The electronic transition energy is 51.5 kcal/mol (555.16 nm) for field-free triplet **I** of $(C_{20}F_{20})_3\&K_2$. Then, W is close to this transition energy but only 6.1 kcal/mol lower than it. This

difference of 6.1 kcal/mol may mainly come from the interaction between two electrons.

The μ_x value also increases enormously when going from field-free triplet triplet **I** of $(C_{20}F_{20})_3\&K_2$ to electrified ones (**III**').

Stabilities and spin states

By comparing the total energies for field-free **I** of $(C_{20}F_{20})_3\&K_2$ in different spin states (see Table 4 Figure 7), it is found that, at CAM-B3LYP/6-31G(2d) level, the triplet and OS singlet structures are, respectively, 8.72 and 1.44 kcal/mol in energy lower than the corresponding CS singlet one. In addition, the energy results at CAM-B3LYP-D3/6-31G(d) level can give the similar order. Therefore, owing to different localizations of two excess electrons, the triplet structure with two single-excess-electrons inside two cages (**1** and **2**) is thermodynamically more stable than both CS and OS singlet ones with lone pair of excess electrons inside middle cage (**2**) for field-free **I** of $(C_{20}F_{20})_3\&K_2$. So, the triplet structure is the ground state for field-free **I** of $(C_{20}F_{20})_3\&K_2$.

It is worth noticing that, results in Figure 7 and Table 4 show that the energies of triplet **I** of $(C_{20}F_{20})_3\&K_2$ under both $F_x < 111 \times 10^{-4}$ and $F_x > -120 \times 10^{-4}$ au are lower than that of CS singlet one, while the CS singlet $(C_{20}F_{20})_3\&K_2$ under both $F_x \geq 111 \times 10^{-4}$ and $F_x \leq -120 \times 10^{-4}$ au are lower in energy than the triplet one. Also, the energies of OS singlet **I** of $(C_{20}F_{20})_3\&K_2$ under $5 \times 10^{-4} \leq |F_x| \leq 30 \times 10^{-4}$ are lower than that of triplet one. That is to say, the following spin states of electrified **I** of $(C_{20}F_{20})_3\&K_2$ are ground state: 1) triplet state with the ranges of $-120 \times 10^{-4} < F_x < -30 \times 10^{-4}$ au and $30 \times 10^{-4} < F_x < 111 \times 10^{-4}$ au; 2) CS singlet state with the range of $F_x \geq 111 \times 10^{-4}$ and $\leq -120 \times 10^{-4}$ au; 3) OS singlet state with the ranges of $-30 \times 10^{-4} \leq F_x \leq$ [illegible] 10^{-4} au and $5 \times 10^{-4} \leq F_x \leq 30 \times 10^{-4}$ au.

Considering the electronic stabilities of **I** of $(C_{20}F_{20})_3\&K_2$, we focus on the first and second vertical electron detachment energies (VDE (I) and (II)) in ground state. From Table 4, for the triplet **I** of $(C_{20}F_{20})_3\&K_2$, the VDE (I) and VDE(II) values are 6.61 and 9.34 eV, respectively. These VDEs are far larger than that of the reported solvated dielectron $e_2@C_{20}F_{60}$ structures ((VDEs (I) of 1.720 ~ 2.283 eV and VDEs (II) of 3.959–5.288 eV)),[32] $e_2@(LiF)_n$ (n = 3 ~ 5, 0.221 ~ 1.254 eV (VDE(1))),[45] and dipole bound dianions of [$(PF_5)_3$ ... dropentalene → Ca].[46] Obviously, the triplet **I** of $(C_{20}F_{20})_3\&K_2$ are stable solvated dielectrons. Changing from triplet to singlet **I** of $(C_{20}F_{20})_3\&K_2$, both VDE (I) and VDE(II) values considerably decrease to 4.42 and 8.33 eV as applying the EEF of -120×10^{-4} au in the x-axis direction but significantly increase to 11.56 and 13.14 eV as applying the *EEF* of 110×10^{-4} au in the x-axis direction. Still, the VDE (I) and VDE(II) values of singlet **I** of $(C_{20}F_{20})_3\&K_2$ under $F_x = -120 \times 10^{-4}$ au are far larger than the corresponding ones of reported $e_2@C_{60}F_{60}$ and $e_2@(LiF)_n$, which indicates that the singlet **I** of $(C_{20}F_{20})_3\&K_2$ under $F_x = 111 \times 10^{-4}$ or -120×10^{-4} au may be still stable.

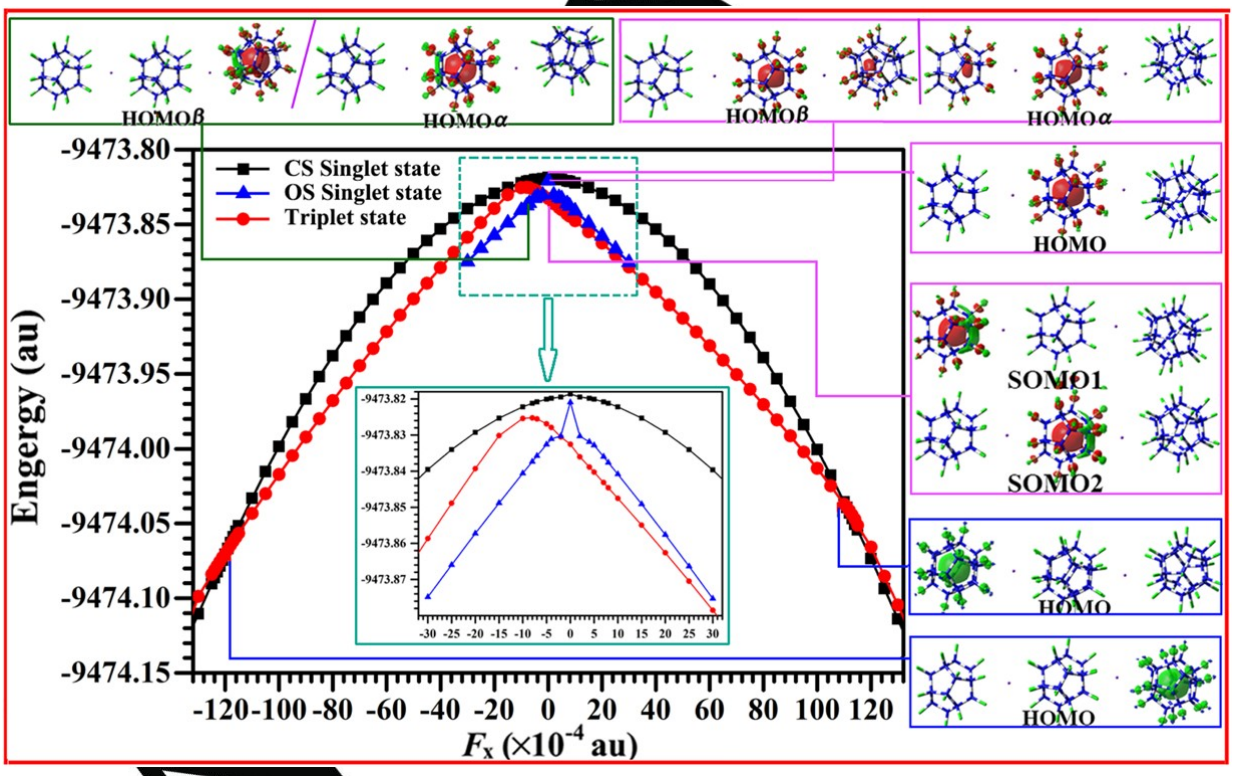

Figure 7. Conversions of spin states of **I** of $(C_{20}F_{20})_3\&K_2$ under OEEFs. Molecular orbitals at the isovalue of 0.004 au.

Table 4. Total energies (E_{tot}, au), relative energies (E_{rel}, kcal/mol), and vertical detachment energies (VDE(I&II), eV).

	Singlet state		Triplet state (T)
	(CS)	(OS)	
$F_x = -120 \times 10^{-4}$ au			

E_{tot}	-9474.070590		-9474.070150
E_{rel}	0.00		0.28 (0.36)[a]
VDE(I)	4.42		
VDE(II)	8.33		
F_x = -20 × 10 $^{-4}$ au			
E_{tot}	-9473.829245	-9473.857273	-9473.839301
E_{rel}	0.00	-17.62 (-17.59)[a]	-6.31 (-6.16)[a]
F_x = 0 au			
E_{tot}	-9473.818630	-9473.820920	-9473.832540
E_{rel}	0.00	-1.44 (-1.07) [a]	-8.72 (-8.59) [a]
VDE(I)			6.61
VDE(II)			9.34
F_x = 20 × 10 $^{-4}$ au			
E_{tot}	-9473.829257	-9473.857629	-9473.862619
E_{rel}	0.00	-15.73 (-17.82) [a]	-20.93 (-20.78) [a]
F_x = 111 × 10 $^{-4}$ au			
E_{tot}	-9747.039340		-0.9747.038810
E_{rel}	0.00		0.33 (-0.27) [a]
VDE(I)	11.56		
VDE(II)	13.14		

[a] results at CAM-B3LYP-D3/6-31G(d) level in brackets.

Conclusion

In this paper, we have presented a new kind of Robin–Day type inter-cage electron-transfer isomers by doping two potassium atoms among three $C_{20}F_{20}$ cages to form peanut-shaped single molecular solvated dielectron $(C_{20}F_{20})_3\&K_2$.

The triplet structure with two single-excess-electrons individually inside left and middle cages (isomers **I** or **II**) is thermodynamically more stable than both CS and OS singlet ones with lone pair of excess electrons inside middle cage (**2**) for field-free $(C_{20}F_{20})_3\&K_2$. Applying an oriented external electric field (OEEF) of -20 × 10^{-4} au (-0.1018 V/Å) or a larger one can result in both left-to-right transfers of the two excess electrons, and then releasing the OEEF can form new kind of inter-cage electron-transfer isomers (**III** or **IV**). Each triplet **I** ~ **IV** with three redox sits may be new members of mixed-valent compounds, namely, Robin-Day Class II.

The lone pair of excess electrons can move from middle $C_{20}F_{20}$ cage to right or left one by applying an OEEF of 111 × 10^{-4} au (0.5705 V/Å) or -120 × 10^{-4} au (-0.6168 V/Å) in the x-axis direction of CS singlet **2** of $(C_{20}F_{20})_3\&K_2$. Applying an OEEF of ±5 × 10^{-4} au (±0.1018 V/Å) in the x-axis direction of CS singlet **I** of $(C_{20}F_{20})_3\&K_2$ can result in one excess electron transfers from middle cage to one end cage.

For electrified **I** of $(C_{20}F_{20})_3\&K_2$, the following spin states are ground state: 1) triplet state in field ranges of -120 × 10^{-4} < F_x < -30 × 10^{-4} au and 30 × 10^{-4} < F_x < 111 × 10^{-4} au; 2) CS singlet state in range of F_x 111 × 10^{-4} and ≤ -120 × 10^{-4} au; 3) OS singlet state in ranges of -30 × 10^{-4} ≤ F_x ≤ -5 × 10^{-4} au and 5 × 10^{-4} ≤ F_x ≤ 30 × 10^{-4} au.

Computational Details

Because of our research systems including long-range interaction and charge transfer, the density functional, coulomb-attenuated hybrid exchange-correlation functional (CAM-B3LYP),[47] is used. It was reported that CAM-B3LYP provides molecular geometries close to experimentally observed structures.[48] In this work, the optimized geometric structures of the $(C_{20}F_{20})_3\&K_2$ with all real frequencies in both singlet and triplet states are obtained at CAM-B3LYP/6-31G(d) level. The spin density distribution and natural population analysis (NPA)[49] of the structures were also obtained at CAM-B3LYP/6-31G(d) level.

Recently, Population and novel hybrid meta exchange-correlation functional M06-2X were successfully used to calculate the vertical electron detachment energy (VDE) of series of excess electron systems.[4,5, 51,52] Therefore, the VDEs of our structures were calculated at M06-2X/6-31G(2d) level, as the following formulas (Cage = $(C_{20}F_{20})_3\&K_2$):

$$\text{VDE (I)} = E[\text{Cage}]^{+}_{opt} - E[\text{Cage}]_{opt} \quad (2)$$

$$\text{VDE (II)} = E[\text{Cage}]^{2+}_{opt} - E[\text{Cage}]^{+}_{opt} \quad (3)$$

The spin contamination is negligible. In the calculations, the expected values of spin eigenvalue $\langle S^2 \rangle$ are 0.0 for [Cage] (singlet) and 2.0 for M^{2+} (triplet), 0.75 for $[Cage]^{+}$, and 0.0 for $[Cage]^{2+}$ species.

The diradical character y_0, which represents a tendency of diradical nature, is obtained on the basis of the UHF spin-unrestricted Hartree–Fock natural orbitals (UNOs):[53]

$$y_0 = 1 - \frac{n_{HOMO} - n_{LUMO}}{1 + \left(\frac{n_{HOMO} - n_{LUMO}}{2}\right)^2} \quad (4)$$

The diradical characters[53] amount to 0% and 100% for closed-shell and pure diradical states, respectively.

In our previous work,[35] it is found that the first transition energy of CIS method is more close to the higher SAC-CI results than the TD-HF, TD-B3LYP, TD-CAM-B3LYP and TD-LC-BLYP results for molecular cluster anion $(FH)_2\{e^-\}(FH)$ and neutral (HCN)···Li with excess electron. Therefore, The CIS/6-31G(d) calculations were performed to obtain the excess electronic absorption spectrum of the $(C_{20}F_{20})_3\&K_2$.

The calculations were performed with the GAUSSIAN program package (GAUSSIAN 09 A02 and D01)[54]. Only the D3-corrected energies were performed with the revision D.01.

Acknowledgements

We acknowledge the financial support from the National Natural Science Foundation of China (Nos. 21662018, and 21764007). This work was also supported by the Science and Technology Project of Jiangxi Provincial Department of Science &Technology (No. 20192BAB203005), and the Natural Science Foundation of Zhejiang Province (No. LQ17E030001).

Keywords: Inter-cage electron-transfer isomers• mixed-valent compound• external electric field • electron localization • DFT

[1] S. Shaik, R. Ramanan, D. Danovich, D. Mandal, *Chem. Soc. Rev*, **2018**, *47*, 5125-5145.

[2] A. Jaroš, E. F. Bonab, M. Straka, C. Foroutan-Nejad, *J. Am. Chem. Soc*, **2019**, *141*, 19644-19654.

[3] A. A. Arabi, C.F. Matta, *J. Phys. Chem. B*, **2018**, *122*, 8631-8641.

[4] Y.-F. Wang, J. Li, J. Huang, T. Qin, Y.-M. Liu, F. Zhong, W. Zhang, Z.-R. Li, *J. Phys. Chem. C,* **2019**, *123*, 23610-23619.

[5] J.-J. Wang, Z.-J. Zhou, H.-M. He, D. Wu, Y. Li, Z.-R. Li, H.-X. Zhang, *J. Phys. Chem. C,* **2016**, *120*, 13656-13666.

[6] C. Foroutan-Nejad, V. Andrushchenko, M. Straka, *Phys. Chem. Chem. Phys*, **2016**, *18*, 32673−32677.

[7] R. M. Young, D. M. Neumark, *Chem. Rev*, **2012**, *112*, 5553-5577.

[8] C. Zhang, Q. Luo, S. Cheng, Y. Bu, *J. Phys. Chem. Lett,* **2018**, *9*, 689-695.

[9] L. Mones, G. Pohlb, L, Turi, *Phys. Chem. Chem. Phys*, **2018**, *20*, 28741-28750.

[10] M. Mauksch, S. B. Tsogoeva, *Phys. Chem. Chem. Phys*, **2018**, *20*, 27740-27744.

[11] L. Das, S. Adhikari, *J. Phys. Chem. B,* **2018**, *122*, 8900-8907.

[12] A. H. C. West, B. L. Yoder, D. Luckhaus, C. Saak, M. Doppelbauer, R. Signorell, *J. Phys. Chem. Lett,* **2015**, *6*, 1487-1492.

[13] S. H. Lin, M. Fujitsuka, T, Majima, T. *Chem. Eur. J,* **2015**, *21*, 16190-16194.

[14] B. Abel, U. Buck, A. L. Sobolewskic, W. Domcke, *Phys. Chem. Chem. Phys*, **2012**, *14*, 22-34.

[15] J. Simons, *J. Phys. Chem. A*, **2008**, *112*, 6401-6511.

[16] J. Fortage, C. Peltier, C. Perruchot, Y. Takemoto, Y. Teki, F. Bedioui, V. Marvaud, G. Dupeyre, L. Pospísil, C. Adamo, M. Hromadová, I. Ciofini, P. P. Lainé, *J. Am. Chem. Soc*, **2012**, *134*, 2691-2705.

[17] P. Delaney, J. C. Greer, *Appl. Phys. Lett,* **2004**, *84*, 431.

[18] Joachim, J. K. Gimzewski, A. Aviram, *Nature*, **2000**, 408, 541-548.

[19] L. L. Tinker, N. D. McDaniel, S. Bernhard, *J. Mater. Chem*, **2009**, 19, 3328-3337.

[20] D. L. Ma, C. M. Che, S. C. Yan, *J. Am. Chem. Soc*, **2009**, *131*, 1835-1846.

[21] I. Amlani, A. O. Orlov, G. Toth, G. H. Bernstein, C. S. Lent, G. L. Snider, *Science*, **1999**, *284*, 289-291.

[22] X. Wang, J. Ma, *Phys. Chem. Chem. Phys*, **2011**, *13*, 16137-16137.

[23] X. Wang, S. Chen, J. Wen, J. Ma, *J. Phys. Chem. C*, **2013**, *117*, 1307-1314.

[24] S. Ito, H. Miura, S. Uchida, M. Takata, K. Sumioka, P. Liska, P. Comte, P. Pechy, M. Graetzel, *Chem. Commun*, **2008**, 5194-5196.

[25] K. Senechal-David, A. Hemeryck, N. Tancrez, L. Toupet, J. A. G. Williams, I. Ledoux, J. Zyss, A. Boucekkine, J. P. Guegan, H. Le Bozec, O. Maury, *J. Am. Chem. Soc*, **2006**, *128*, 12243-12255.

[26] F. Wahl, A. Weiler, P. Landenberger, E. Sackers, T. Voss, A. Haas, M. Lieb, D. Hunkler, J. Wörth, L. Knothe, H. Prinzbach, *Chem. Eur. J*, **2006**, *12*, 6255-6267.

[27] H. F. Bettinger, K. N. Kudin, G. E. Scuseria, *J. Am. Chem. Soc*, **2001**, *123*, 12849-12856.

[28] J. Jia, H.-S. Wu, X.-H. Xu, X.-M. Zhang, H. Jiao, *J. Am. Chem. Soc*, **2008**, *130*, 3985-3988.

[29] O. J. Leighton, M. A. Jones, B. Mosquera, C. S. George, A. R. Mark, *J. Am. Chem. Soc*, **2019**, *141*, 1672-1683.

[30] L. G. Christophorou, J. K. Olthoff, *J. Phys. Chem. Ref. Data*, **2001**, *30*, 449-473.

[31] Y.-F. Wang, Z.-R. Li, D. Wu, C.-C. Sun, F.-L. Gu, *J. Comput. Chem*, **2010**, *31*, 195-203.

[32] Y.-F. Wang, W. Chen, G.-T. Yu, Z.-R. Li, D. Wu, C.-C. Sun, *J. Comput. Chem*, **2011**, *32*, 2012-2021.

[33] Y.-F. Wang, Y. Li, Z.-J. Zhou, Z.-R. Li, D. Wu, J. Huang, F. L. Gu, *ChemPhysChem*, **2012**, *13*, 756-76[illegible]

[34] Y.-F. Wang, J. Huang, G. Zhou, Z.-R. [illegible] *Acta. Phys-Chim. Sin. B*, **2012**, *28*, 2574-2580.

[35] Y.-F. Wang, Z.-R. Li, D. Wu, Y. Li, C.-C. [illegible], F L. [illegible] *Phys. Chem. A*, **2010**, *114*, 11782-11787.

[36] Y.-F. Wang, Z.-R. Li, D. Wu, [illegible] C.-C. Sun, F L. Gu, *J. Phys. Org. Chem,* **2017**, *30*, e3625.

[37] Y. Bai, Z.-J. Zhou, J.-[illegible], Y. Li, D. [illegible] W. Chen, Z.-R. Li, C.-C. Sun, *J. Phys. Chem.*, **2013**, *117*, 2835-2843.

[38] Z.-B. Liu, Y.-C. Li, J.-J. Wang, Y. Bai, D. Wu, Zhi-Ru Li, *J. Phys. Chem. A*, **2013**, *117*, 6674-6686.

[39] M. B. Robin, P. [illegible], *Adv. Inorg. Chem. Radiochem*. **1967**, *10*, 247-422.

[40] C. Creutz, H. Taube, *J. Am. Chem. Soc*. **1969**, *91*, 3988-3989.

[41] K. D. Demadis, C. M. Hartshorn, T. J. Meyer, *Chem. Rev*. **2001**, *101*, 2655-2685.

[42] C. Lambert, G. Nöll, *J. Am. Chem. Soc.* **1999**, *121*, 8434-8442.

[43] S. F. Nelsen, *Chem. Eur. J*. **2000**, *6*, 581-588.

[44] N. Sadlej-Sosnowska, *Phys. Chem. Chem. Phys*, **2015**, *17*, 23716-23719.

[45] L. Zhang, S. Yan, F. L. Gu, Y. Bu, *J. Phys. Chem. B*, **2008**, *112*, 3767-3772.

[46] P. Skurski, J. Simons, J. Chem. Phys, **2000**, *112*, 6563.

[47] P. A. Limacher, K. V. Mikkelsen, H. P. Luthi, *J. Chem. Phys*, **2009**, *130*, 194114.

[48] J. E. Carpenter, F. Weinhold, *J Mol Struct: THEOCHEM*, **1988**, *169*, 41-62.

[49] K. Szalewicz and B. Jeziorski, *J. Chem. Phys*., **1999**, *109*, 1198.

[50] Y. Zhao, D. G. Truhlar, *Theor. Chem. Acc*, **2008**, *120*, 215−241.

[51] L. Li, J. Feng, F. L. Gu, C. Zhu, *ChemistrySelect*, **2018**, *3*, 12782-12790.

[52] J. Hou, Y. Liu, X. Zhang, Q. Duan, D. Jiang, J. Qin, *New J. Chem*, **2018**, *42*, 1031-1036.

[53] K. Kamada, K. Ohta, A. Shimizu, T. Kubo, R. Kishi, H. Takahashi, E. Botek, B. Champagne, M. Nakano, *J. Phys. Chem. Lett*. **2010**, *1*, 937-940.

[54] M. J. Frisch, G. W. Trucks, H. B. Schlegel, G. E. Scuseria, M. A. Robb, J. R. Cheeseman, J. A. Montgomery Jr., T. Vreven, K. N. Kudin, J. C. Burant, J. M. Millam, S. S. Iyengar, J. Tomasi, V. Barone, B. Mennucci, M. Cossi, G. Scalmani, N. Rega, G. A. Petersson, H. Nakatsuji, M. Hada, M. Ehara, K. Toyota, R. Fukuda, J. Hasegawa, M. Ishida, T. Nakajima, Y. Honda, O. Kitao, H. Nakai, M. Klene, X. Li, J. E. Knox, H. P. Hratchian, J. B. Cross, V. Bakken, C. Adamo, J. Jaramillo, R. Gomperts, R. E. Stratmann, O. Yazyev, A. J. Austin, R. Cammi, C. Pomelli, J. W. Ochterski, P. Y. Ayala, K. Morokuma, G. A. Voth, P. Salvador, J. J. Dannenberg, V. G. Zakrzewski, S. Dapprich, A. D. Daniels, M. C. Strain, O. Farkas, D. K. Malick, A. D. Rabuck, K. Raghavachari, J. B. Foresman, J. V. Ortiz, Q. Cui, A. G. Baboul, S. Clifford, J. Cioslowski, B. B. Stefanov, G. Liu, A. Liashenko, P. Piskorz, I. Komaromi, R. L. Martin, D. J. Fox, T. Keith, M. A. Al−Laham, C. Y. Peng, A. Nanayakkara, M. Challacombe, P. M. W. Gill, B. Johnson, W. Chen, M. W. Wong, C. Gonzalez, J. A. Pople, GAUSSIAN 09, revision A.02, Gaussian, Inc., Pittsburgh PA, **2009**.